Journal of ELECTRONIC MATERIALS, Vol. 44, No. 3, 2015
DOI: 10.1007/s11664-014-3618-z

Effect of Substrate Temperature on the Properties of Sprayed WO_3 Thin Films Using Peroxotungstic Acid and Ammonium Tungstate: A Comparative Study

V.V. GANBAVLE,[1] J.H. KIM,[2] and K.Y. RAJPURE[1,3]

1.—Electrochemical Materials Laboratory, Department of Physics, Shivaji University, Kolhapur 416004, India. 2.—Department of Materials Science and Engineering, Chonnam National University, 300 Yongbong-Dong, Buk-Gu, Gwangju 500-757, South Korea. 3.—e-mail: rajpureky@gmail.com

A comparative study on the physicochemical properties of tungsten oxide (WO_3) thin films synthesized using peroxotungstic acid (PTA) and ammonium tungstate (AT) by simple spray pyrolysis technique is reported. X-ray diffraction patterns show that the films deposited using both the precursors are polycrystalline with monoclinic crystal structure. The x-ray photoelectron spectroscopy studies confirm that the films are sub-stoichiometric with O/W ratios of 2.93 and 2.87, respectively, for typical PTA and AT films. Tungsten (W) exists in two chemical states, 5+ and 6+. Scanning electron microscopy images show the uniform and dense network of wires in PTA films, while the films deposited using AT possess a porous structure with small grains. Electrical and dielectric studies show that films are highly resistive and possess high dielectric constant. The near ultra-violet, blue, green and weak red emissions due to defects were observed in the photoluminescence studies. Properties of the WO_3 thin films reported here are suitable for gas sensor applications. Films deposited using PTA are more functional than those deposited using AT.

Key words: Thin films, spray pyrolysis, WO_3, photoluminescence, x-ray photoelectron spectroscopy (XPS), electrical properties

INTRODUCTION

Controlled growth of semiconductors for the design of gas sensors has become an area of immense interest. The application of semiconducting tungsten oxide (WO_3) is spreading over a wide range of areas such as electrochromism, electrophotocatalysts, gas sensors, light-emitting diodes and for hydrogen production.[1–6] Much of the earlier work focused on electrochromism of WO_3. Nowadays, WO_3 is being used as a gas sensing material for oxidizing as well as reducing gases. As the structure and properties of the thin film are significantly different from its bulk phase, it is worth making an attempt to study the transformations in physicochemical properties of thin films with respect to preparative parameters. It is well known that the properties and applications of low-dimensional materials such as thin films and nanostructures are mainly governed by the crystal structure, chemical composition, surface morphology, chemical and thermal stability, porosity, and phase stability of the resulting structures, and the preparation conditions.[7–9] Several thin film deposition techniques such as sputtering,[7] solution thermolysis,[9] chemical vapor deposition,[10] thermal evaporation,[11] spray pyrolysis,[12,13] etc. have been used to synthesise WO_3 thin films. Microstructure modeling provides an idea that the morphology of a gas sensor must show a high proportion of surface atoms to bulk atoms for better responses by the sensors.[14,15] The factors influencing the sensitivity of a gas sensor include grain size and charge carrier

(Received February 6, 2014; accepted December 31, 2014; published online January 15, 2015)

concentration of the material,[16,17] which decide the probable application and efficiency of the material. Qin et al.[18] prepared a network of WO_3 nanowires for sub-ppm and ppb level nitrogen dioxide (NO_2) sensing at a low operating temperature (125°C). Single crystalline potassium-doped WO_3 nanosheets were synthesized simply by heating foil of tungsten (W), and high sensitivity towards H_2S and acetone was reported by Zhang et al.[19] A scalable and general route for synthesizing nanowires of titanium oxide, tin oxide, zinc oxide, copper oxide and tungsten oxide for gas nanosensors has been reported. The nanowires were synthesized via sputter deposition of correlative metals over single walled porous carbon nanotube templates followed by oxidation. The response towards N_2 and H_2 detection at different operating temperatures was tested.[20] NO_2 sensing properties of the sensors based on solvothermal synthesis of $W_{18}O_{49}$ nanowires and nanorods were investigated over 100–250°C operating temperature for gas concentrations ranging from 1 ppm to 20 ppm.[21] A high response was achieved at 150°C operating temperature and the maximum is observed for nanowires rather than nanorods due to the high specific surface area.

In the present study, we report the comparative studies on the physicochemical properties of WO_3 thin films synthesized using two precursors, peroxotungstic acid (PTA) and ammonium tungstate (AT) by the spray pyrolysis technique. Also, the effect of substrate temperature on the physicochemical properties of the films was simultaneously carried out.

EXPERIMENTAL

Materials Synthesis

WO_3 thin films were synthesized using two precursors, AT and PTA, by a simple cost-effective spray pyrolysis technique. AT was prepared by dissolving tungstic acid (H_2WO_4, 0.187 g) (S.D. Fine Chemicals, Mumbai, India) in 20 mL of ammonia solution (NH_4OH) (Thomas Bakers) at 80°C, and then it was diluted to 10 mM concentration. 0.5 M PTA was prepared by dissolving W metal powder (Loba Chimie , Mumbai, India) in 30 mL of hydrogen peroxide (H_2O_2, 30%). This solution was kept in an ice bath for 1 h to control the exothermic reaction. Then, it was rigorously stirred for 48 h at room temperature until all the powder was completely dissolved. The PTA thus formed was then diluted to 10 mM using double-distilled water. Colorless AT and yellow-colored PTA solution were then separately sprayed onto the preheated corning glass substrates at different temperatures ranging from 400°C to 475°C in a locally fabricated spray deposition system. All other optimized parameters of the spray deposition, such as nozzle to substrate distance (28 cm), solution concentration (10 mM), solution quantity (75 mL) and spray rate (4.5 mL/min), etc., were kept constant.

Material Characterization

To identify the crystal structure, thin films were characterized by x-ray diffraction (XRD) technique and the diffraction patterns were recorded using a Rigaku Miniflex II x-ray diffractometer using Cu K_α radiation of wavelength 1.5406 Å. A monochromatic x-ray beam of energy 1253.6 eV was used for the x-ray photoelectron spectroscopy (XPS) study (XPS; Physical Electronics PHI 5400, USA) of the films to obtain information about the chemical composition and valence state of the elements. Surface morphology and topography of the films were studied using scanning electron microscopy (SEM; Model JEOL JSM-6701F, Japan) and atomic force microscopy (AFM; Digital Instrument, Nanoscope III). Absorption spectra obtained from a UV–Visible spectrophotometer (UV–Vis Spectrophotometer, Shimadzu) was used to calculate the optical band gap. To study the defects in the thin films, room temperature photoluminescence (PL) spectra were recorded using a Perkin-Elmer luminescence spectrometer (model: LS55). Electrical and dielectric measurements were performed using the Keithley 6514 electrometer and LCR meter (HP 4284-A), respectively. Thickness of the films was measured using surface profiler (XP-1 Stylus Profiler; Ambios Technology). Thermoelectric power was measured to check the type of electrical conductivity of the films.

RESULTS AND DISCUSSION

Reaction Mechanism

WO_3 thin films were deposited using two precursor solutions, AT and PTA, prepared using H_2WO_4 and W metal powder in respective solvents. AT (10 mM) was prepared by dissolving H_2WO_4 in ammonium hydroxide at 80°C until a clear solution was formed. The suggested chemical reaction is as follows:

$$H_2WO_4 + 2NH_4OH \xrightarrow{80^\circ C} (NH_4)_2WO_4 + 2H_2O \quad (1)$$

AT was then sprayed onto the preheated glass substrates to form WO_3 thin films. Solvent evaporation and thermal decomposition of AT along the temperature gradient in the spray deposition system resulted into WO_3 formation[22]:

$$(NH_4)_2WO_4 \xrightarrow{\Delta} WO_3 + 2NH_3 \uparrow + H_2O \uparrow \quad (2)$$

PTA was prepared by dissolving 3.04 g of W metal powder in 30 mL of H_2O_2 (30%) in an ice bath to control exothermic reaction, and then stirred for 48 h until a clear yellowish solution was formed. Finally, the solution was diluted to 10 mM

concentration. The PTA was formed as $WO_3{\cdot}n\,H_2O_2{\cdot}mH_2O$ and the value of n and m could be determined by iodometric titration and TG analysis.[13] Pyrolytic decomposition of PTA occurs on the substrate to form WO_3. The chemical reactions involved in the synthesis are as follows:

$$W + H_2O_2 + H_2O \xrightarrow{\text{stirring}} WO_3.nH_2O_2.mH_2O + \Delta \quad (3)$$

$$WO_3.nH_2O_2.mH_2O \xrightarrow{\Delta} WO_3 + H_2O + O_2 \uparrow \quad (4)$$

Usually, when n is less than 0.1, PTA precipitates as yellow colloids, which is not acceptable in the spray pyrolysis technique.[13] Typically, partial decomposition occurs within the aggregates of the precursor solution by the evaporation of the solvent in the air due to the temperature gradient. Nucleation and growth of the film starts when the partially decomposed residue reaches the substrate and subsequent crystallization results in crystalline WO_3 thin films.

X-ray Diffraction Studies

Crystal structure and phase identification of WO_3 thin films were carried out using XRD analysis. Figure 1 shows the XRD patterns of thin films deposited at different substrate temperatures. The XRD patterns of the films match well with standard data (JCPDS card no. 43-1035), confirming the monoclinic crystal structure. Intensity of the XRD peaks is lower for the film deposited at 400°C due to the insufficient thermal energy required for decomposition. When the deposition temperature was increased to 425°C, the intensity of diffraction peaks increased and further decreased for higher substrate temperatures (450°C and 475°C). At higher substrate temperature, the solution decomposes before reaching the substrate surface due to the high thermophoretic force which results in decrease of the film thickness. AT films show intense doublet oriented along the (020) and (200) planes while PTA films show a preferred orientation along the (200) plane. Crystallite size was calculated using the Debye–Scherer formula[23] and is presented in Table I along with the corresponding thickness of the films. Crystallite size is least for the

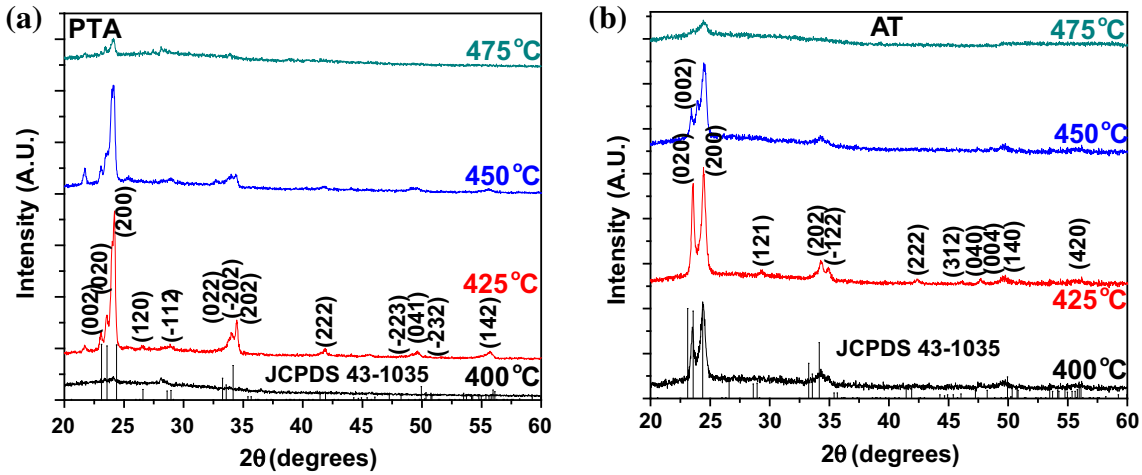

Fig. 1. X-ray diffraction patterns of (a) PTA- and (b) AT-based WO_3 thin films deposited at various substrate temperatures.

Table I. Crystallite size, thickness and roughness values for WO_3 thin films deposited at different substrate temperatures using PTA and AT

	Crystallite size (nm)		Thickness (nm)		RMS roughness (nm)	
Substrate temperature (°C)	PTA	AT	PTA	AT	PTA	AT
400	33	30	596	415	50	61
425	34	28	481	351	79	89
450	37	34	390	232	19	47
475	41	49	289	91	16	25

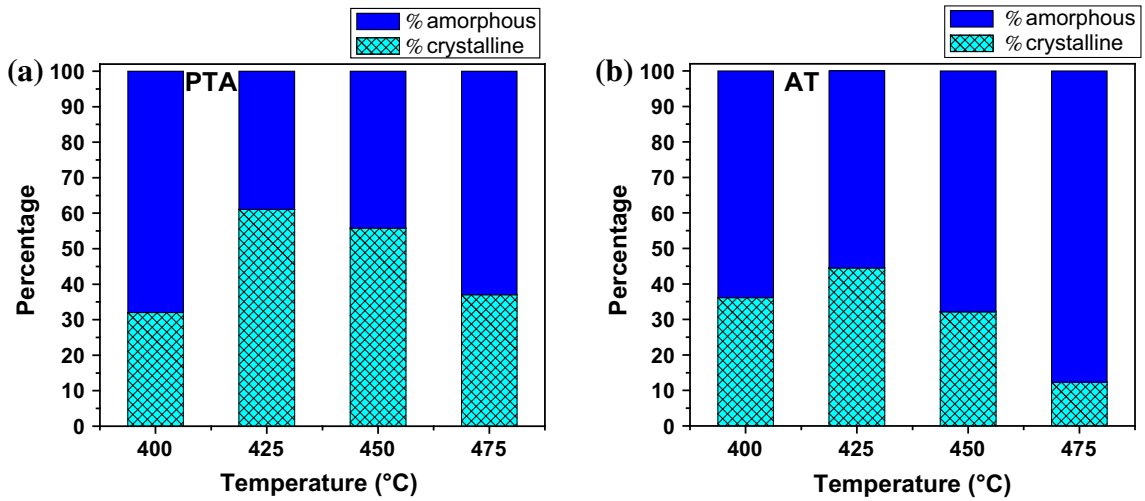

Fig. 2. Variation of crystalline and amorphous components with substrate temperature for (a) PTA- and (b) AT-based WO_3 thin films.

film deposited at 425°C substrate temperature, and it is seen to be increasing at higher substrate temperatures.

The crystalline component in thin films is one of the critical parameters determining the behavior of the films. Figure 2 shows the percentage of crystalline and amorphous components of the films with respect to substrate temperature. The maximum crystalline component is observed for the films deposited at 425°C. Thus, we conclude that the optimum temperature for the formation of highly crystalline monoclinic WO_3 thin films is 425°C. The percentage of the crystalline component was measured using formula[24]:

$$\%C = (\text{area under the curve}/\text{total area}) \times 100 \quad (5)$$

where *area under the peak* is the summation of the area under all the XRD peaks and *total area* is the area under the complete XRD pattern. We have calculated % C by considering the peaks within the 2θ range of 20°–60°. Before calculating the percentage of the crystalline component, an empty background run was subtracted in order to get the utmost accurate value of the crystalline and amorphous components. The crystalline component in the films is increased up to a substrate temperature of 425°C and then decreased thereafter, as seen in Fig. 2. This is attributed to the decrease in film thickness at higher substrate temperatures which in turn decreases the crystalline component.[25]

X-ray Photoelectron Spectroscopy

Survey and detailed scan x-ray photoelectron (XP) spectra for the W 4*f*, O 1*s* of AT- and PTA-based WO_3 thin films deposited at 425°C substrate temperatures are shown in Fig. 3. The quantitative analysis is carried out by survey scan XP spectra for identifying the elements and their stoichiometry. The observed O/W ratio is 2.87 and 2.93 for the AT and PTA films, respectively. Survey scan spectra of the AT and PTA films show various peaks belonging to the core levels of the W, O, C and Auger electron transitions. The appearance of a peak at 975 eV in both spectra is due to OKLL Auger electrons transition. The appearances of binding energy (BE) peaks of hydroxyl groups, surface oxygen or especially of carbonates is common, as seen in Ref. 26. Here, the C 1*s* BE line is used as an internal standard for the estimation of the value of the peak position. C 1*s* is present due to the contamination during sample handling before XPS measurement.[26] BE peaks of various core levels of W confirm that W is present in the oxidized state.[27,28] BE values of the core levels are in good agreement with that of the sub-stoichiometric WO_3. Table II lists the BE values of subshells of the fourth orbit of W. These values are higher than those for elemental W and less than that for stoichiometric WO_3. This removes the possibility of the existence of W in metallic state and indicates that WO_3 films have oxygen vacancies, while the same is confirmed from the PL studies. It is also noticed from the PL studies that the density of oxygen deficiency is larger for the AT-based films than that for the PTA-based films. The doublet separation for different core levels of W for both precursors is in accordance with the reported values.[27,28]

Figure 3b and c show narrow scan XP spectra of the W 4*f* core level of PTA- and AT-based films deposited at 425°C. The relative peak positions of the elements are decided by the chemical state of those elements. Small chemical shifts can cause overlapping of the peaks of different states of elements. To deal with small chemical shifts and overlapped peaks of the 4*f* doublet, we deconvoluted the peaks and used Gaussian fitting by subtracting the Shirley background. The appearance of two 4*f* doublets of W in the XP spectra for both types of films is indicative of two valence states, i.e. W^{5+} and

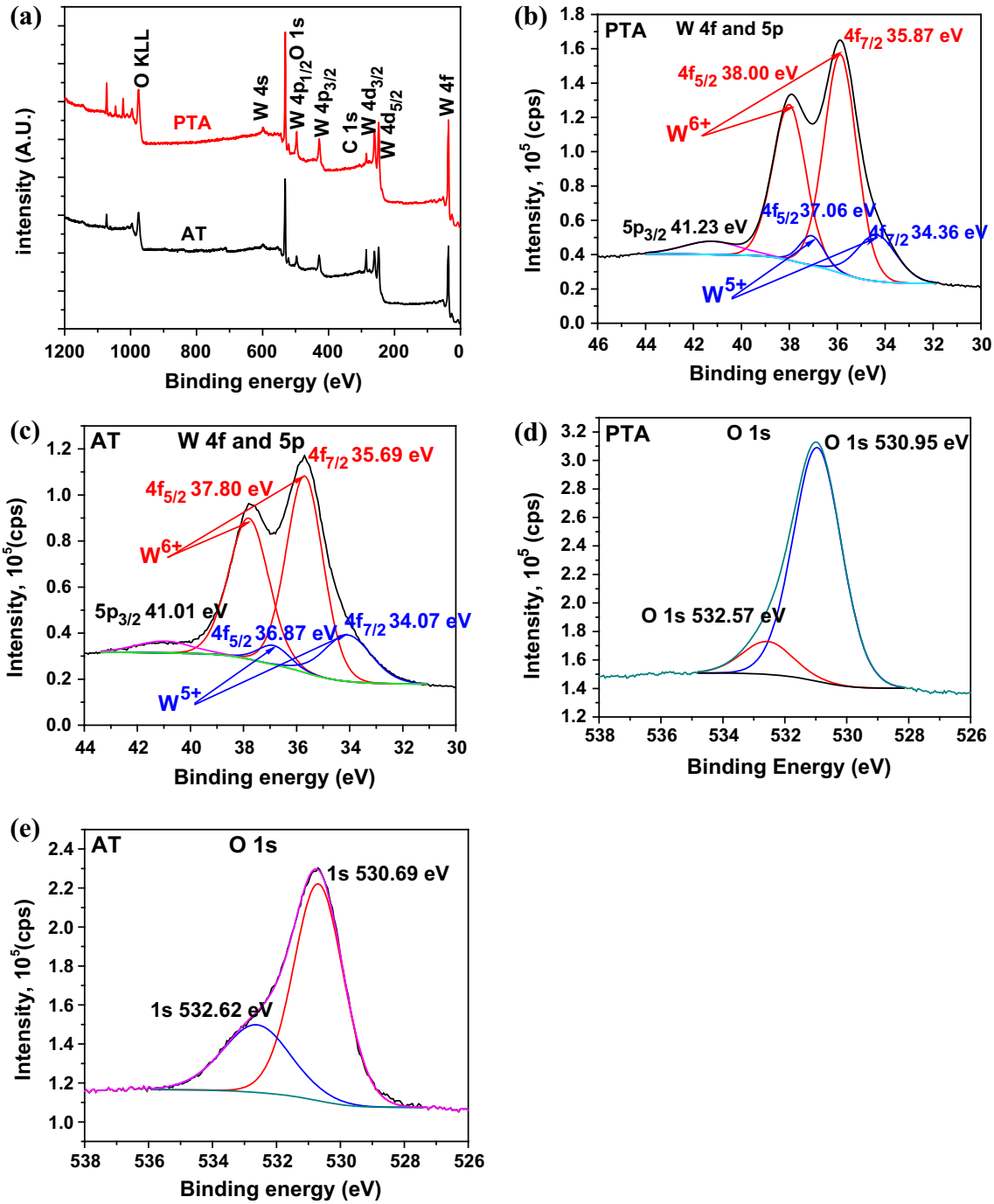

Fig. 3. (a) Survey scan XP spectra of WO_3 thin films deposited at 425°C. (b) Narrow scan XP spectrum of the 4*f* fine structure state of W of PTA- and (c) AT-deposited WO_3 thin films. (d) Narrow scan XP spectrum of oxygen, O 1*s* fine structure state of PTA- and (e) AT-deposited WO_3 thin films.

W^{6+}. The ratio of the area under the curve of W^{5+} to that of W^{6+} was calculated and it is 0.18 for PTA- and 0.21 for AT-based films, respectively.

The narrow scan deconvoluted XP spectra of O 1*s* core level of PTA- and AT-based films are shown in Fig. 3d and e, respectively. A distinctly asymmetric peak having broad linewidth with a shoulder at the higher BE side is observed for both the spectra. This result is due to the adsorption of water onto the surface whose component is obtained by deconvoluting the spectra. The peak at the lower energy level is assigned to the O bonded to W[29] and that at the higher energy value is assigned to the adsorbed water[30] on the film surface.

Table II. Comparison of the observed BE values with W and WO_3 for WO_3 thin films deposited using different substrate temperatures and observed chemical shifts

		Observed BE values (eV)					Chemical shift from WO_3 (eV)			
		AT		PTA			AT		PTA	
Core level	W (eV)	W + 5	W + 6	W + 5	W + 6	WO_3 (eV)	W + 5	W + 6	W + 5	W + 6
$4f_{7/2}$	31.4	34.07	35.70	34.36	35.87	36.2	2.13	0.50	1.84	0.33
$4f_{5/2}$	33.6	36.87	37.80	37.06	38.00	38.1	1.23	0.30	1.04	0.10
$4d_{5/2}$	243.5	–	248.20	–	247.90	248.5	–	0.30		0.60
$4d_{3/2}$	255.9	–	259.20	–	259.15	259.2	–	0.0		0.05
$4p_{3/2}$	423.6	–	428.00	–	428.00	428.0	–	0.00		0.00
$4p_{1/2}$	490.4	–	496.88	–	496.92	496.98	–	0.10		0.06
$4s$	594.3	–	598.56	–	598.66	598.7	–	0.14		0.04

Scanning Electron Microscopy

Figure 4 reveals a uniform microstructure (inset of Fig. 4c and d) of networked wires of 1–4 μm length for PTA- and AT-based films. These wires are densely grown and randomly distributed all over the surface. The solution droplets continuously collide and decompose onto the substrate surface. Consistent overlapping of the droplets onto each other form a wire-like morphology with the wires separated at a distance of the diameter of the drop size. Further, the images highlight that the grains emerging out on the wires are larger in number for the AT-based films as compared to the PTA-based films. AT-deposited thin films show uniformly deposited homogeneously dispersed wires and grains, whereas for PTA small numbers of grains are seen to cling to the wires. A dual scale structure is observed for the PTA-based films (at higher magnification) with the secondary wired structure possessing rods of different diameters having lengths around 1 μm. The disoriented network of wires makes the films porous. For the AT-based films, a dual scale structure is rarely observed at a few sites. WO_3 films deposited using PTA show a more dense structure than those deposited using AT. Structure densification occurring in the PTA-deposited films can be attributed to the acidic environment of the resulting solvent, enhancing the growth rate of the films. One common thing observed in both types of films is that, with the increase in substrate temperature, the density of the wire-network structure increased up to 425°C, making the films compact. Films deposited at higher substrate temperatures, i.e., at 450°C and 475°C, have morphological differences for both types of films, which is also seen in AFM studies. At lower substrate temperatures, the grain size is around 0.5 μm, whereas for the film deposited at higher substrate temperatures it is 0.1 μm. Spherical grains on the wires are observed for the AT films, while for PTA films no overgrown grains are visible.

Atomic Force Microscopy

The topography of the films was examined by AFM, recorded in tapping mode on a 3 × 3 μm^2 scan area (Figs. 5, 6). Root mean square roughness (R_q) is presemted in Table I. The roughness and grain size of the films is observed to depend on the deposition temperature and the choice of the precursor. Considerable differences are found in the values of roughness of the films deposited using PTA and AT. Films having a high roughness value have large effective surface areas which is a key factor for gas sensor material. It is observed that R_q increases initially up to 400°C substrate temperature and then decreases with further increases in temperature above 425°C. Improved morphology and grain growth is observed for the film deposited at 425°C substrate temperature (Figs. 5b, 6b). This is due to the availability of more nucleation centers at relatively higher thermal energy. R_q is higher for the film deposited at 425°C. Some overgrown grains can be observed from the spikes in the whitish regions in the films deposited at lower temperature. This is due to the incomplete decomposition and slow growth rate of the films at lower substrate temperatures.

Optical Studies

Optical absorption spectra were recorded in the 300–1100 Å wavelength range and analyzed using Tauc's plot to measure the band gap of the films. Figure 7 shows the absorption spectra of the WO_3 thin films with the insets showing the graphs of $(\alpha h\nu)^{1/2}$ versus $h\nu$. It can be seen from the Fig. 7 that the optical absorption decreases with increase in deposition temperature. The decrease in absorbance for both types of films (PTA- and AT-based) at high substrate temperatures is attributed to the decrease in the film thickness. Further, as the surface roughness decreases at elevated deposition temperatures, the scattering losses are also reduced. The absorption values for AT-deposited films are

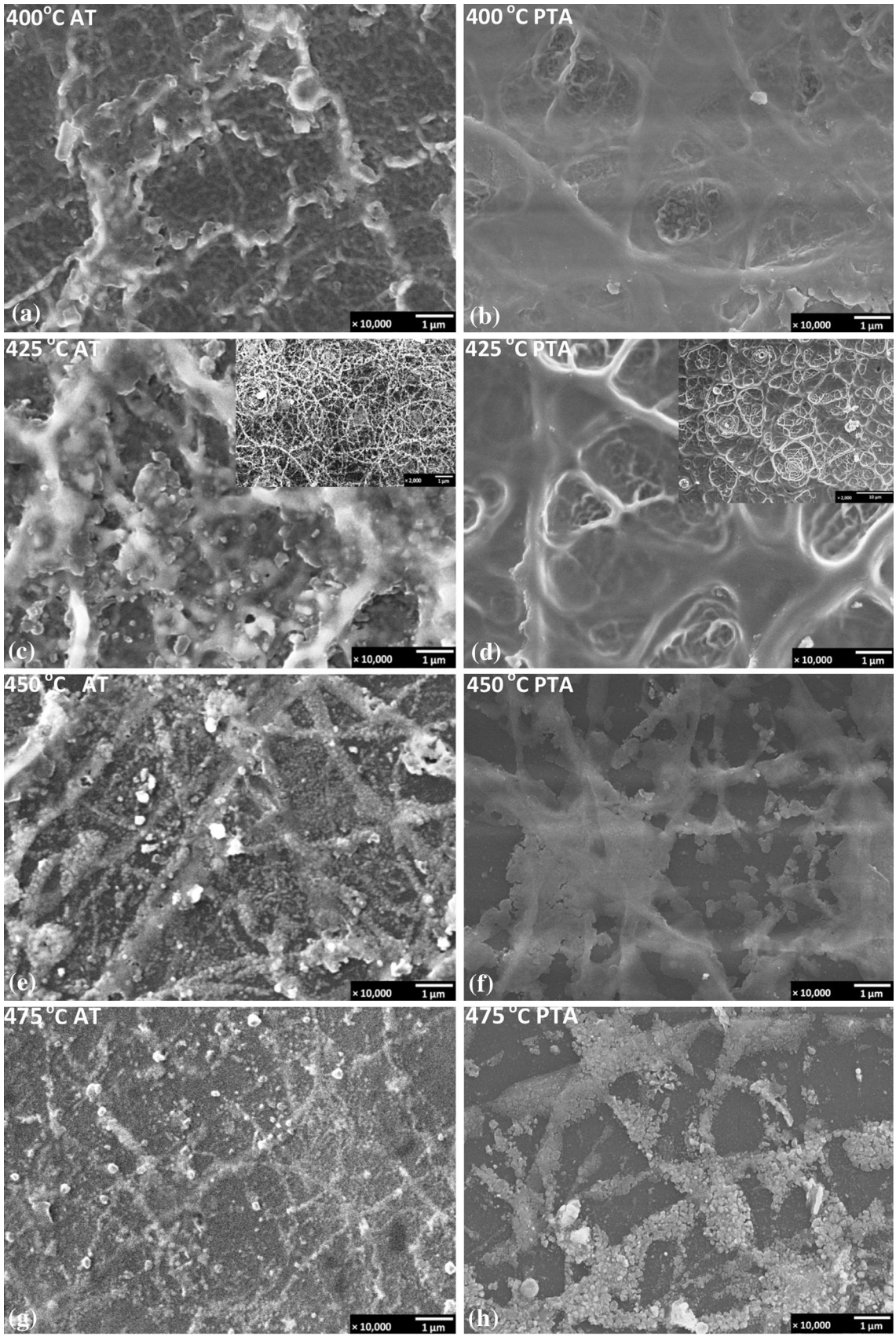

Fig. 4. SEM images of the WO_3 films deposited at (a) 400°C, (c) 425°C, (e) 450°C, and (g) 475°C using PTA, and (b) 400°C, (d) 425°C, (f) 450°C, and (h) 475°C using AT. Insets of (c) and (d) show lower magnification images.

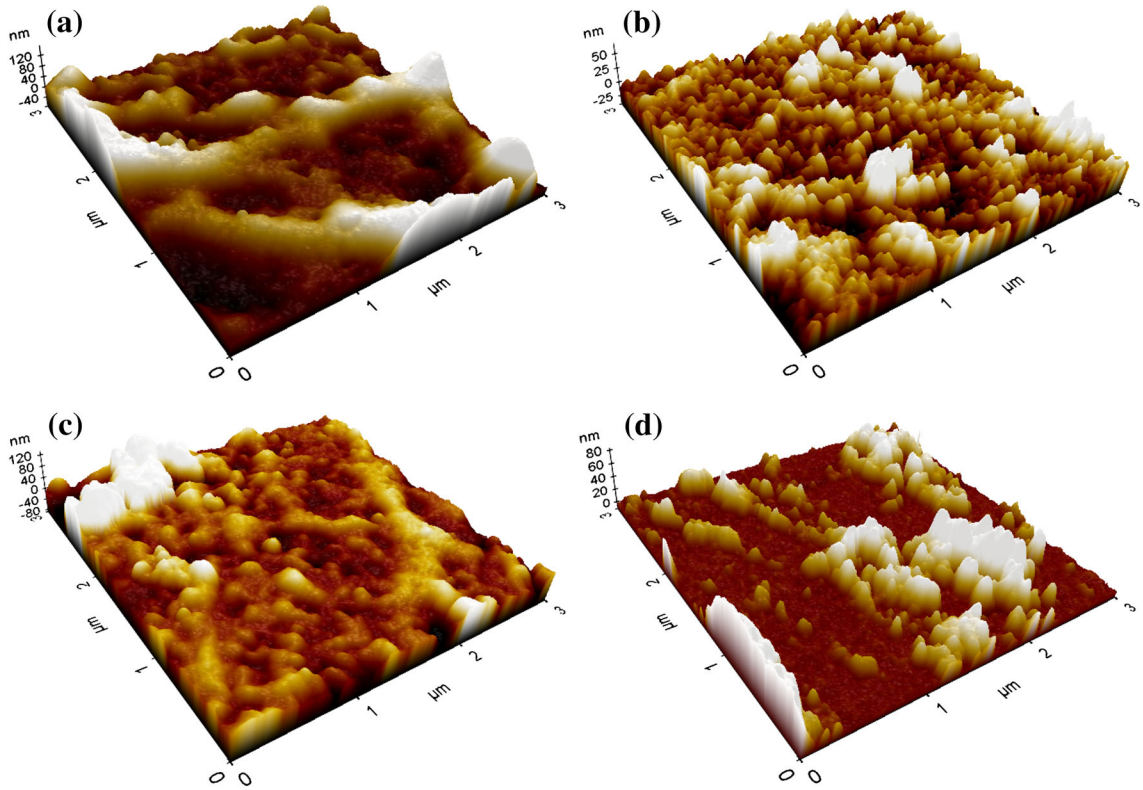

Fig. 5. Three-dimensional AFM images of the WO_3 films deposited at (a) 400°C, (b) 425°C, (c) 450°C, and (d) 475°C using AT.

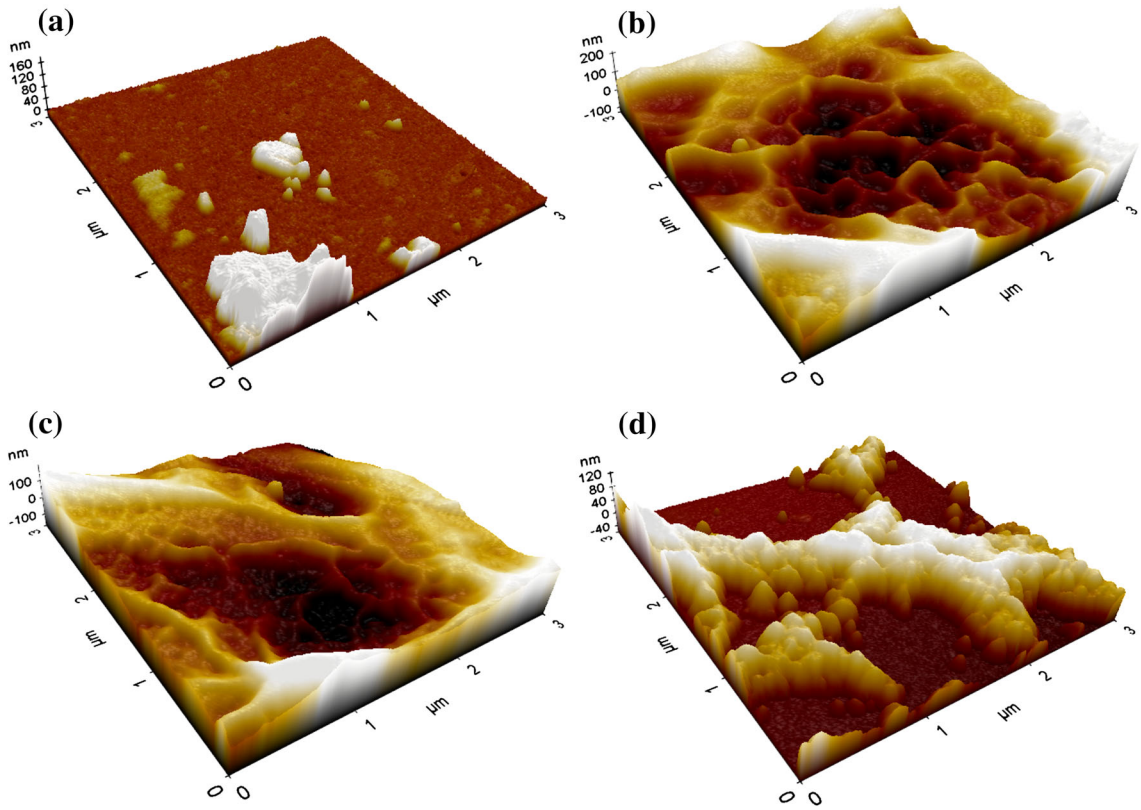

Fig. 6. AFM images of the WO_3 films deposited at (a) 400°C, (b) 425°C, (c) 450°C, and (d) 475°C using PTA.

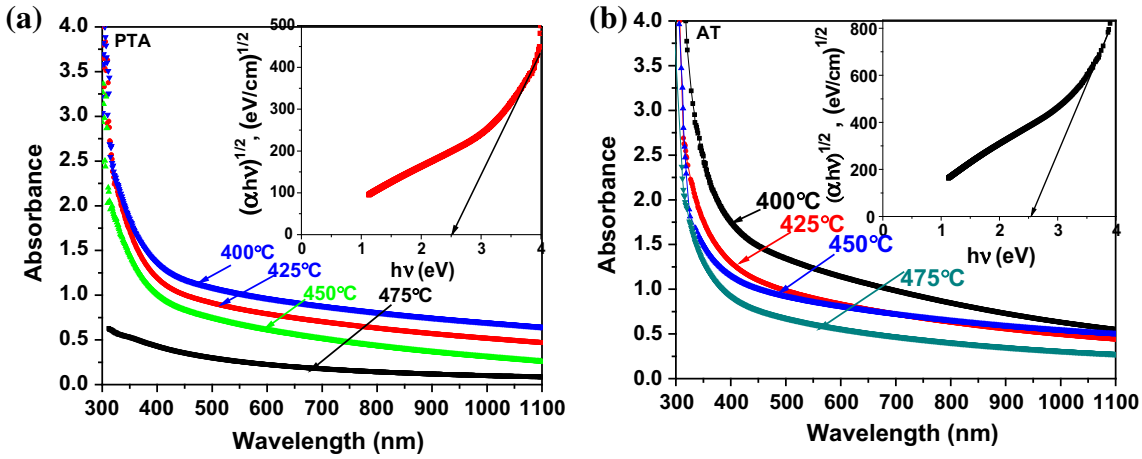

Fig. 7. (a) The optical absorbance spectra of WO_3 thin films prepared at different temperatures using (a) PTA and (b) AT. Insets show plots of $(\alpha h\nu)^{1/2}$ versus photon energy ($h\nu$) for typical film deposited at 425°C.

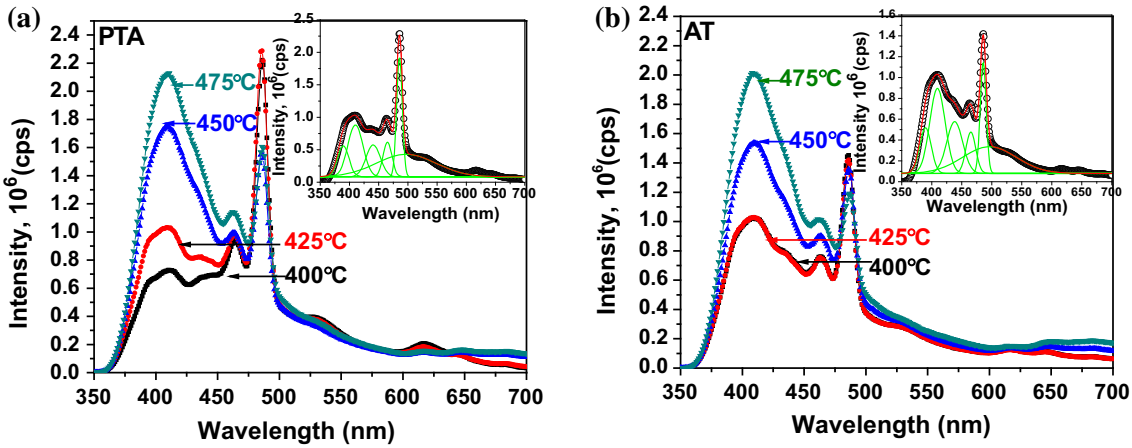

Fig. 8. PL spectra of WO_3 thin films deposited at various substrate temperatures using (a) PTA (b) AT. Insets show deconvoluted Guassian fitted PL spectra of the film deposited at 425°C.

higher than for PTA films. In contrast, the thickness of the AT films is lower than that of PTA films. The sharp increase in the absorbance of the films at 350 nm wavelength is due to the fundamental absorption edge of WO_3. Also, it can be seen that the absorption edge is slightly shifted towards a lower wavelength with increases in substrate temperature, probably due to the band tailing effect.[31] The measured band gap values are in good agreement with the literature values. Slight variations of the band gap with respect to substrate temperature can be seen due to the variation in stoichiometry. Band gap values of the PTA-based films are higher than for the AT-based films. A more compact microstructure would have caused the higher band gap for the PTA-based films.[32]

Visible PL at room temperature has been the focus of numerous studies, which have revealed information about the types and density of defects.[33] Figure 8 shows the PL spectra of the PTA and AT films excited by 325 nm wavelength, and the insetd show deconvoluted fitted PL spectra of the typical WO_3 thin films. Individual contributions of the near ultra-violet (NUV), red, blue and green color in the PL spectra is determined by deconvoluting and Gaussian fitting the peaks. It shows various emissions corresponding to various electrons transitions within the different types of defects. Similar types of defects are observed for both types of films. NUV emission peaks at the wavelengths 389 nm and 410 nm are due to the deep level oxygen vacancies in the WO_3 structure. It is normally observed that defects, especially oxygen vacancies, play a key role in deciding the gas sensing properties of the films. A fully oxidized surface is less susceptible than the surface with oxygen deficiencies (WO_{3-x}). Vacancies are commonly known to generate localized states near the fundamental band gap, either in the

valence band or in the conduction band. A fall in the intensity of the NUV peak indicates a decrease in the density of oxygen deficiency with an increase in substrate temperature. These vacancies in WO_3 can generate three types of defect states, a hyperdeep one associated with the *s*-like bonding band, a high-lying one associated with the *s*-like antibonding band, and a donor state associated with the valence bands near the fundamental band gap.[34] It is also noted that, with a decrease in the intensity of NUV peaks, peak intensity corresponding to band to band transition at the wavelength of 485 nm is increased. Major differences observed in spectra are differences in the intensity of the band to band transition, which is relatively higher for the PTA films than the AT films. Similarly, the intensity of peaks due to oxygen vacancy are more than the band to band transition for AT films and vice versa for PTA films. Besides this, a blue emission at the wavelength of 466 nm, 496 nm was also observed.[35] Very weak red transitions due to the monovalent ions (H^+) at the interstitial sites were observed at 616 nm and 643 nm wavelengths. Tables III and IV list peak wavelengths and contributions of the peak in the

Table III. Wavelengths of peak value of fitted PL spectra of WO_3 thin films deposited using PTA and AT

	Area under the peak (%)											
	PTA						AT					
Substrate temperature (°C)	p1	p2	p3	p4	p5	p6	p1	p2	p3	p4	p5	p6
400	9.3	26.5	25.2	6.8	10.1	22.0	9.7	25.3	16.2	8.0	13.1	27.6
425	8.9	26.9	25.7	6.9	10.3	22.1	10.1	25.3	16.1	7.9	12.8	27.8
450	9.2	25.4	26.7	6.8	9.3	22.6	8.9	25.2	27.4	7.3	9.0	22.0
475	9.2	26.5	28.1	7.1	8.0	21.0	8.22	26.0	32.2	7.9	6.0	19.3

Table IV. Components of the peak of fitted PL spectra of WO_3 thin films deposited using PTA and AT

	Wavelength of peak (nm)											
	PTA						AT					
Substrate temperature (°C)	p1	p2	p3	p4	p5	p6	p1	p2	p3	p4	p5	p6
400	389	410	446	465	486	500	389	409	438	465	486	496
425	389	410	441	465	486	497	390	409	438	465	486	496
450	389	411	443	465	486	495	389	407	433	466	486	495
475	389	412	444	466	486	493	389	406	434	466	487	494

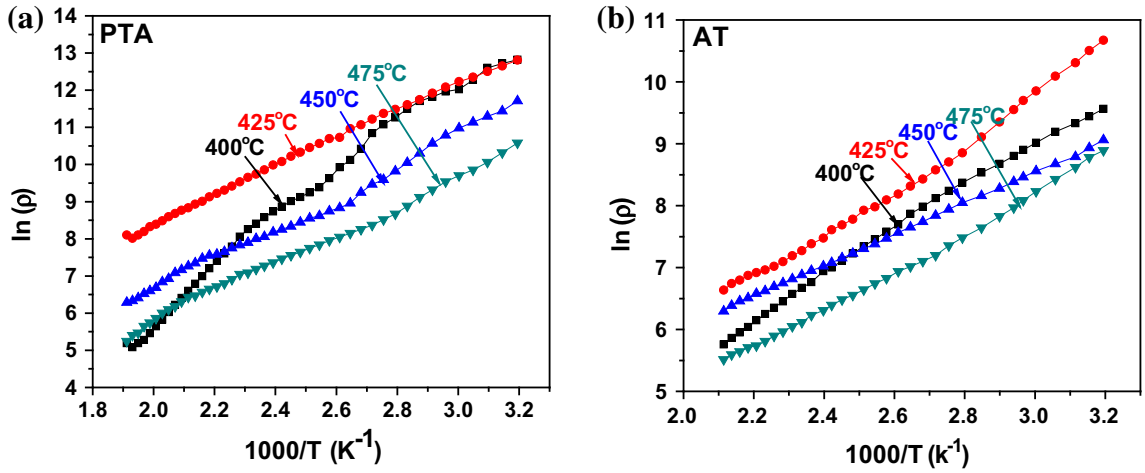

Fig. 9. Variation of resistivity with respect to temperature for the films deposited at different temperatures using (a) PTA and (b) AT.

emission spectra, hence indicating the density of the defects. No measurable shift can be observed in the peak position of the films for the band to band transition and the deep level NUV transitions. For other transitions, a slight shift is observed for both types of films.

Electrical Resistivity

Measurements of the electrical resistivity can be considered as a mean to monitor the electrical properties of the films. In general, the electronic transport in transition-metal oxides can be understood by the hopping conduction mechanism of majority carriers (electrons) through the oxygen vacancies. We observed variations in the values of resistivity of the WO_3 films deposited using PTA and AT. The nature of the graphs of ln ρ versus 1000/T (Fig. 9a and b) reveals the semiconducting behavior of the thin films. As per the XPS studies, the ratio of the W^{5+}/W^{6+} is higher for AT (0.21) than PTA (0.18), giving rise to more free electrons and thereby reducing the electrical resistivity of the AT-based films. The activation energies calculated for the PTA- and AT-based films deposited at different substrate temperatures are shown in Table V.

Table V. Activation energy of WO_3 thin films deposited at different substrate temperatures using PTA and AT

	Activation energy (eV)	
Substrate temperature (°C)	**PTA**	**AT**
400	0.55	0.30
425	0.32	0.31
450	0.35	0.21
475	0.32	0.26

Dielectric Constant

Dielectric measurements of WO_3 thin films with respect to frequency at room temperature are shown in Fig. 10. Dielectric constant decreases rapidly at lower frequencies and remains nearly constant at higher frequencies, showing the dispersion of the dielectric constant at lower frequencies. The dielectric constant for the AT-based films is higher than that for PTA-based films. The dielectric constant at higher frequencies decreases when the jumping frequency of electric charge cannot follow the alternations of the applied electric field beyond a certain critical frequency. At higher frequencies, the losses are reduced and the dipoles contribute to polarization.[36]

CONCLUSIONS

The n-type sub-stoichiometric WO_3 thin films having wire-network-like morphology were synthesized by a simple cost-effective spray pyrolysis technique. The effect of substrate temperatures on the properties of WO_3 films deposited using two precursors, AT and PTA, are reported. The comparative study showed strong orientation of the crystallites along the (2 0 0) plane for PTA-based films which possess more crystalline components than AT-based films. W exists in W^{6+} and W^{5+} chemical states, inducing bonding defects. The results indicate that parameters such as crystalline component, crystallite size, roughness, thickness, morphology, absorption edge and oxygen vacancies strongly depend on the substrate temperature. The optimum substrate temperature for highly crystalline WO_3 thin films is 425°C. Various defects with different densities belonging to NUV, band to band, and blue and weak red emissions were observed from PL studies. Large variations in the resistivity values of the PTA- and AT-based films were observed indicating that PTA-based films are more resistive than AT-based ones; while the dielectric

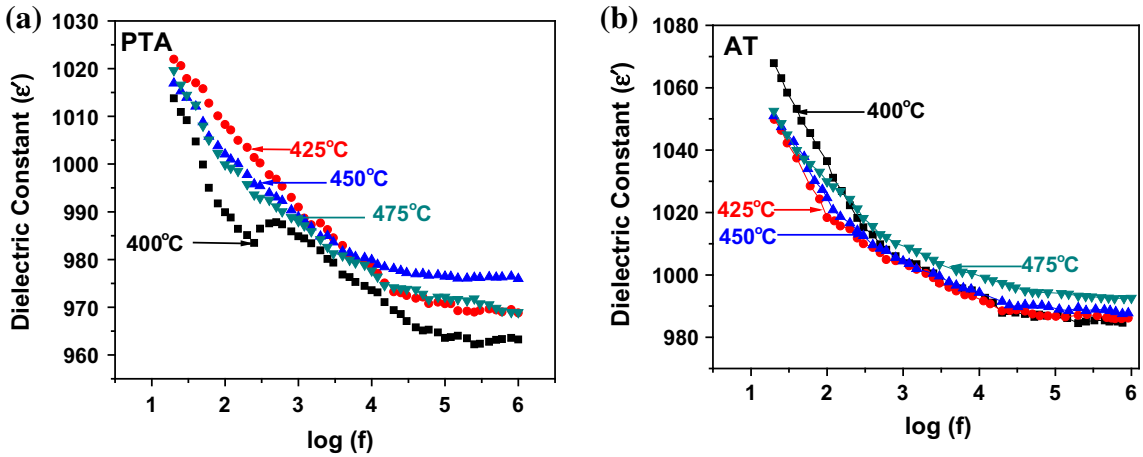

Fig. 10. Variation of dielectric constant with respect to frequency at various substrate temperatures using (a) PTA and (b) AT.

constant is higher for AT-based films compared to PTA-based films. The active surface area for the PTA-deposited films is apparently more than the AT-deposited films. In conclusion, PTA is found to be a more suitable precursor than AT to obtain crystalline and sub-stoichiometric WO_3 thin films for their probable application as gas sensors.

ACKNOWLEDGEMENTS

One of the authors, Mr. V.V. Ganbavle is very grateful to UGC, New Delhi, for providing financial support through a UGC-BSR junior research fellowship. This work is partly supported by UGC through financial support under a major research project entitled "Photocatalytic degradation of waste water using sprayed tungsten trioxide (WO_3) thin films", No. 41-869/2012. We acknowledge D. Haranath, CSIR-NPL, New Delhi, for providing PL measurements, and Michael Neumann-Spallart, CNRS France, for discussions and suggestions.

REFERENCES

1. M. Zadsar, H.R. Fallah, M.H. Mahmoodzadeh, and S.V. Tabatabaei, *J. Lumin.* 132, 992 (2012).
2. A. Boudiba, P. Roussel, C. Zhang, M.G. Olivier, R. Snyders, and M. Debliquy, *Sensors Actuat. B* 187, 84 (2013).
3. M. Ranjbar, S. Fardindoost, S.M. Mahdavi, A. Iraji zad, and N. Tahmasebi, *Sol. Energ. Mat. Sol. C* 95, 2335 (2011).
4. W. Chu and Y.F. Rao, *Chemosphere* 86, 1079 (2012).
5. M.Z. Ahmad, A.Z. Sadek, M.H. Yaacob, D.P. Anderson, G. Matthews, V.B. Golovko, and W. Wlodarski, *Sensors Actuat. B* 179, 125 (2013).
6. J.M.O. Leon, D.R. Acosta, U. Pal, and L. Castaneda, *Electrochim. Acta* 56, 2599 (2011).
7. R.A. Batchelor, M.S. Burdis, and J.R. Siddle, *J. Electrochem. Soc.* 143, 1050 (1996).
8. O. Bohnke, C. Bohnke, A. Donnadieu, and D. Davazoglou, *J. Appl. Electrochem.* 18, 447 (1988).
9. P.R. Patil, S.H. Pawar, and P.S. Patil, *Solid State Ionics* 136, 505 (2000).
10. J.H. Yun, B.Y. Kim, and S.W. Rhee, *Thin Solid Films* 312, 259 (1998).
11. J.D. Musgraves, N. Carlie, J. Hu, L. Petit, A. Agarwal, L.C. Kimerling, and K.A. Richardson, *Acta Mater.* 59, 5032 (2011).
12. B.W. Mwakikunga, E.S. Haddad, A. Forbes, and C. Arendse, *Phys. Status Solidi A* 205, 150 (2008).
13. C.Y. Kim, S.G. Cho, S. Parka, and D.K. Choi, *J. Ceram. Process. Res.* 10, 851 (2009).
14. D.E. Williams and K.F.E. Pratt, *J. Chem. Soc. Faraday Trans.* 94, 3493 (1998).
15. S. Kirkpatrick, *Rev. Mod. Phys.* 45, 574 (1973).
16. J. Tamaki, Z. Zhang, K. Fujimori, M. Akiyama, T. Harada, N. Miura, and N. Yamazoe, *J. Electrochem. Soc.* 141, 2207 (1994).
17. X. Wang, S.S. Yee, and W.P. Carey, *Sensors Actuat. B* 24, 454 (1995).
18. Y. Qin, F. Wang, W. Shen, and M. Hu, *J. Alloy. Compd.* 540, 21 (2012).
19. B. Zhang, J. Liu, S. Guan, Y. Wan, Y. Zhang, and R. Chen, *J. Alloy. Compd.* 439, 55 (2007).
20. N.D. Hoa, V.V. Quang, D. Kim, and N.V. Hieu, *J. Alloy. Compd.* 549, 260 (2013).
21. Y. Qin, X. Li, F. Wang, and M. Hu, *J. Alloy Compd.* 509, 8401 (2011).
22. P.R. Patil and P.S. Patil, *Thin Solid Films* 382, 13 (2001).
23. B.D. Cullity, *Elements of X-ray diffraction*, 3rd ed. (Boston: Addison-Wesley Publishing Inc., 1956), pp. 261–262.
24. P.S. Prevey, *J. Therm. Spray Technol.* 9, 369 (2000).
25. S. Thanikaikarasan, T. Mahalingam, A. Kathalingam, Y.D. Kim, and T. Kim, *Vacuum* 83, 1066 (2009).
26. S.S. Shinde and K.Y. Rajpure, *J. Alloy. Compd.* 509, 4603 (2011).
27. R. Nyholm, A. Berndtsson, and N. Martensson, *J. Phys. C* 13, L1091 (1980).
28. W. Grunert, E.S. Spiro, R. Feldhaus, K. Anders, G.V. Antoshin, and K.M. Minachev, *J. Catal.* 107, 522 (1987).
29. I.M. Szilagyi, I. Sajo, P. Kiraly, G. Tarkanyi, A.L. Toth, A. Szabo, K. Varga-Josepovits, J. Madarasz, and G. Pokol, *J. Therm. Anal. Calorim.* 98, 707 (2009).
30. A.R. Babar, S.S. Shinde, A.V. Moholkar, C.H. Bhosale, J.H. Kim, and K.Y. Rajpure, *J. Alloy Compd.* 509, 3108 (2011).
31. A. Subrahmanyam and A. Karuppasamy, *Sol. Energ. Mat. Sol. C* 91, 266 (2007).
32. R.S. Vemuri, M.H. Engelhard, and C.V. Ramana, *Appl. Mater. Interfaces* 4, 1371 (2012).
33. E. Orhan, M.A. Santos, M.A. Maurera, F.M. Pontes, C.O. Paiva-Santos, A.G. Souza, J.A. Varela, P.S. Pizani, and E. Longo, *Chem. Phys.* 312, 1 (2005).
34. SZh Karazhanov, Y. Zhang, A. Mascarenhas, S. Deb, and L.W. Wang, *Solid State Ionics* 165, 43 (2003).
35. C. Shi, Y. Wei, X. Yang, D. Zhou, C. Guo, J. Liao, and H. Tang, *Chem. Phys. Lett.* 328, 1 (2000).
36. V.S. Sawant, S.S. Shinde, R.J. Deokate, C.H. Bhosale, B.K. Chougule, and K.Y. Rajpure, *Appl. Surf. Sci.* 255, 6675 (2009).